Prediction of Structures, Properties, and Functions of Alternating Copolymers of Ethylene Imine and Ethylene Oxide As an Example of Molecular Design for Polymers

Yuji Sasanuma,* Ryota Kumagai, and Kohji Nakata

Department of Applied Chemistry and Biotechnology, Faculty of Engineering, Chiba University, 1-33 Yayoi-cho, Inage-ku, Chiba 263-8522, Japan

Received June 6, 2006; Revised Manuscript Received July 2, 2006

ABSTRACT: Conformational analysis of two alternating copolymers, poly(ethylene imine-*alt*-ethylene oxide) (PEIEO) and poly(*N*-methylethylene imine-*alt*-ethylene oxide) (PMEIEO), has been carried out by the inversional−rotational isomeric state (IRIS) analysis of ab initio molecular orbital (MO) calculations and ^{1}H and ^{13}C NMR experiments for their model compounds. On the basis of the conformational energies derived therefrom and molecular mechanics and MO calculations, higher-order structures, physical properties, and functions of the two copolymers have been predicted as an example of molecular design. These copolymers are expected to form various hydrogen bonds: PEIEO, N−H···O (interaction energy, −1.75 kcal mol^{-1}), C−H···N (−0.68 kcal mol^{-1}), and C−H···O (−0.21 kcal mol^{-1}); PMEIEO, C−H···N (−0.66 kcal mol^{-1}), and C−H···O (−0.41 kcal mol^{-1}). In particular, the N−H···O hydrogen bond of PEIEO is too strong to be broken even by protic solvents such as methanol and water but replaced by an intermolecular N−H···O═S attraction in dimethyl sulfoxide. The C−N and C−O bonds of PEIEO prefer the trans state as found for poly(ethylene imine) (PEI) and poly(ethylene oxide), whereas the C−C bond does not have its own conformational preference and its conformational equilibrium is determined only by the hydrogen bond strength (HBS). The characteristic ratio of PEIEO largely depends on HBS: 1.5 (HBS = 100%); 6.5 (0%). In contrast, the weak hydrogen bonds of PMEIEO little affect the characteristic ratio; 5.2 (HBS = 100%); 5.9 (0%). According to Mattice's analysis (*Macromolecules* **2004**, *37*, 4711), PEIEO and PEI tend to form circular paths due to the intramolecular hydrogen bonds. Both molecular mechanics calculations using the Amber force field and density functional MO calculations under the periodic boundary condition have suggested that a double-helical structure may be formed in the PEIEO crystal. The possibility that these copolymers will be utilized as gene carriers and ion conductors is discussed, and the synthetic method is also suggested. In conclusion, these copolymers should be promising and deserve to be synthesized.

1. Introduction

Molecular design for polymers may be to predict the atomic arrangement, i.e., the primary structure that actualizes such higher-order structures, physical properties, and functions as one desires. To this end, it is significant to elucidate correlations between primary structures, higher-order structures, and properties of polymers and to predict structures, properties, and functions of nonexistent polymers and encourage polymer chemists to challenge syntheses of the new polymers.

So far, we have interpreted conformational characteristics of polymers including heteroatoms such as oxygen, sulfur, nitrogen, and silicon in terms of intramolecular and intermolecular interactions, using their monomeric and oligomeric model compounds,[1−3] and found that the unperturbed and crystallized polymers have the same conformational preferences as the models. The solution and thermal properties of the polymers have been elucidated from ab initio molecular orbital (MO) calculations and NMR experiments for the models and the rotational isomeric state (RIS) scheme for the polymers. For polyimines, we have developed the inversional−rotational isomeric state (IRIS) scheme,[4,5] by which the configurational and conformational equilibrium can be discussed in accordance with statistical mechanics. Our studies have suggested the possibility that a given polymer may be fully characterized by means of its model compound(s) even though the polymer itself has not been synthesized.

Poly(ethylene imine) (PEI) and poly(ethylene oxide) (PEO), respectively, form N−H···N and (C−H)···O intramolecular hydrogen bonds,[4,6] which essentially determine their conformational characteristics and spatial configurations. Because of the electron donor properties, both PEI and PEO have been used as solid polymer electrolytes[7] and gene delivery polymers.[8,9] In vivo, PEI is protonated,[10] basic, and cytotoxic, whereas PEO is neutral, water-soluble, and biocompatible. To enhance water solubility and reduce cytotoxicity, PEI has often been copolymerized with PEO to yield PEI-*block*-PEO and PEI-*graft*-PEO.[11,12] It is true that these copolymers are not so cytotoxic as PEI alone, but the hydrophilic PEO block covers the particle surface and masks the PEI block, and hence the transfection efficiency is reduced. Recently, alternating copolymers of oligomers of ethylene imine and ethylene oxide have been prepared and found to be less cytotoxic than PEI and more efficient in transfection than PEI-*block*-PEOs.[13] If the two oligomers could be reduced to one monomeric unit, we would obtain the alternating copolymer, poly(ethylene imine-*alt*-ethylene oxide) ($[-NH(CH_2)_2O(CH_2)_2-]_x$, PEIEO, see Figure 1). The alternating copolymer may exhibit unique properties and functions. To our knowledge, there was an attempt to synthesize PEIEO from *N*-(2-hydroxyethyl)aziridine,[14] but the molecular weight was as small as 267 (corresponding to the trimer).

* To whom correspondence should be addressed. E-mail: sasanuma@faculty.chiba-u.jp. Fax: +81 43 290 3394.

10.1021/ma0612531 CCC: $33.50
Published on Web 08/11/2006

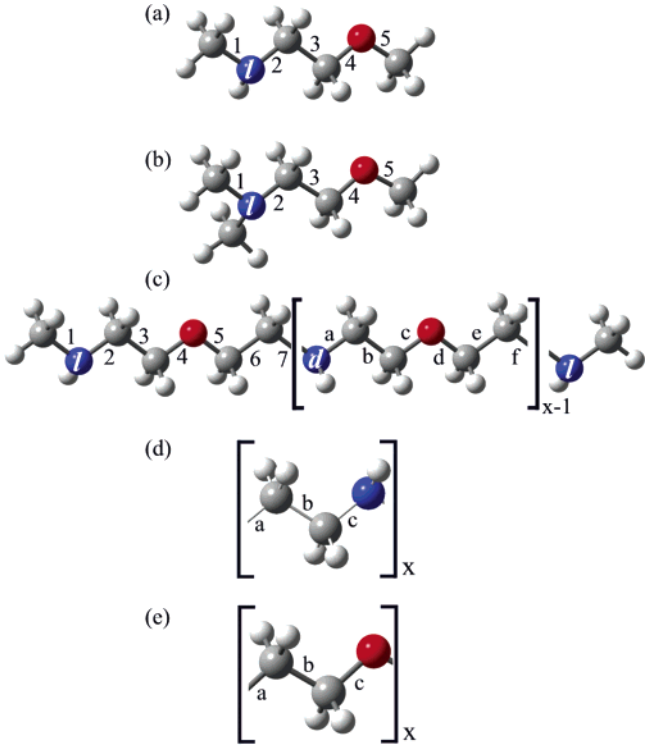

Figure 1. All-trans states of (a) *N*-(2-methoxyethyl)methylamine (MEMA), (b) *N*,*N*-(2-methoxyethyl)dimethylamine (MEDA), (c) poly(ethylene imine-*alt*-ethylene oxide) (PEIEO), (d) poly(ethylene imine) (PEI), and (e) poly(ethylene oxide) (PEO). As indicated, the bonds are designated. The *l* and *d* forms are defined as follows. For example, PEIEO in the all-trans state is put on paper as shown. When the hydrogen atom of the most left-hand NH group appears on this (that) side of the paper, the nitrogen site is considered to adopt the *d* (*l*) form. For other nitrogen sites, the *d* and *l* configurations are defined similarly. The *dd* and *ll* forms are referred to as *meso*, and *dl* and *ld* as *racemo*. The all-trans *meso* and *racemo* forms have the two NH hydrogen atoms on the same and opposite sides, respectively. If the NH hydrogen atoms of PEIEO are replaced by methyl groups, the resultant polymer corresponds to poly(*N*-methylethylene imine-*alt*-ethylene oxide) (PMEIEO).

This study has dealt with *N*-(2-methoxyethyl)methylamine ($CH_3NH(CH_2)_2OCH_3$, MEMA) and *N*,*N*-(2-methoxyethyl)dimethylamine ($(CH_3)_2N(CH_2)_2OCH_3$, MEDA) as model compounds of PEIEO and its *N*-methyl substituted polymer, poly(*N*-methylethylene imine-*alt*-ethylene oxide) ($[-N(CH_3)(CH_2)_2O-(CH_2)_2-]_x$, PMEIEO), to derive the conformational energies from ab initio MO calculations and NMR experiments and investigate intramolecular interactions formed in the copolymers. Conformational characteristics, higher-order structures, and physical properties of the two polymers have been predicted by the IRIS calculations using the energy parameters and molecular mechanics and MO calculations. In this paper, the results are discussed in comparison with those for PEI and PEO, and their applications and synthetic methods are also discussed.

2. Computations and Experiments

2.1. Ab Initio MO Calculations. Ab initio MO calculations were carried out with the Gaussian03 program[15] installed on an HPC Silent-SCC T2 computer. For each conformer of MEMA or MEDA, the geometrical parameters were fully optimized at the HF/6-31G-(d) level, and the thermal correction to the Gibbs free energy (at 25 °C and 1 atm) was calculated with a calibration factor of 0.9135.[16] With the optimized geometry, the self-consistent field (SCF) energy was computed at the MP2/6-311++G(3df, 3pd) level. All the SCF calculations were performed under the tight convergence. The Gibbs free energy was calculated from the SCF and thermal-correction energies, being given here as the difference from that of the all-trans conformer and denoted as ΔG_k (k: conformer number).

Ab initio MO calculations including the counterpoise correction[17,18] at the MP2/6-311+G(3df, 2p) level were carried out for MEMA−dimethyl sulfoxide (DMSO) complexes. The complex geometries were fully optimized, and the intermolecular interaction energies were estimated by the natural bond orbital (NBO) analysis.[19,20] The crystal structure of PEIEO was predicted for by the geometrical optimization at the B3LYP/6-31G(d) level under the periodic boundary condition.[21,22]

2.2. Molecular Mechanics Calculations. Molecular mechanics calculations were performed to search for the optimum crystal structure of deca(ethylene imine-*alt*-ethylene oxide) using the Amber8 program[23] installed on an HPC-IAXP8 computer. The ff99 forced field[24] was employed, together with the restrained electrostatic potential (resp) atomic charges[25] derived from MO calculations at the B3LYP/6-31G(d) level for the oligomers. The full conjugate gradient minimization of the total energy was performed with the Sander module of the Amber8 program.

2.3. Sample Preparation. *N*-(2-Methoxyethyl)methylamine was purchased from Aldrich and used without further purification. *N*,*N*-(2-Methoxyethyl)dimethylamine was prepared by a condensation between 2-chloro-*N*,*N*-dimethylethylamine and sodium methoxide.[26] A cyclic compound to derive vicinal coupling constants for the NMR analysis, 2-methylmorpholine (2MM), was prepared as follows. 1-Amino-2-propanol and 2-chloroethanol were condensed with sodium carbonate to yield *N*-(2-hydroxyethyl)-2-hydroxypropylamine.[27] The product was cyclized by an intramolecular condensation using sulfuric acid to give 2MM.[28]

2.4. NMR Measurements. ^{1}H (^{13}C) NMR spectra were measured at 500 MHz (126 MHz) on a JEOL JNM-LA500 spectrometer equipped with a variable temperature controller in the Chemical Analysis Center of Chiba University. During the measurement, the probe temperature was maintained within ±0.1 °C fluctuations. The $\pi/2$ pulse width, data acquisition time, and recycle delay were 5.6 (5.0) μs, 3.3 (2.0) s, and 3.7 (2.0) s, respectively. Here, the values in the parentheses represent the ^{13}C NMR parameters. In the ^{13}C NMR measurements, the gated decoupling technique was employed. Before the Fourier transform, zero filling was conducted so that the digital resolution would be smaller than 0.01 Hz. The solvents were cyclohexane-d_{12} (C_6D_{12}), chloroform-*d* ($CDCl_3$), methanol-d_4 (CD_3OD), dimethyl-d_6 sulfoxide ($(CD_3)_2SO$ or DMSO-d_6), and deuterium oxide (D_2O), and the solute concentration was ca. 5 vol %. The NMR spectra were simulated with the gNMR program[29] to obtain the chemical shifts and coupling constants.

3. Results and Discussion

3.1. ^{1}H NMR. Figure 2 shows ^{1}H NMR spectra observed from methylene protons of MEMA. The simulations gave two vicinal coupling constants, $^3J_{HH}$ (= $^3J_{AB}$ = $^3J_{A'B'}$) and $^3J'_{HH}$ (= $^3J_{AB'}$ = $^3J_{A'B}$), as listed in Table 1. The observed coupling constants can be expressed as

$$^3J_{HH} = {}^3J_G^{HH}\, p_t^{CC} + \frac{{}^3J'_T{}^{HH} + {}^3J''_G{}^{HH}}{2}\, p_g^{CC} \qquad (1)$$

and

$$^3J'_{HH} = {}^3J_T^{HH}\, p_t^{CC} + \frac{{}^3J'_G{}^{HH} + {}^3J''_G{}^{HH}}{2}\, p_g^{CC} \qquad (2)$$

where $^3J_T^{HH}$'s and $^3J_G^{HH}$'s are defined in Figure 3, and p_t^{CC} and p_g^{CC} are trans and gauche fractions of the C−C bond, respectively. Therefore, we have

$$p_t^{CC} + p_g^{CC} = 1 \qquad (3)$$

As $^3J^{HH}$'s in eqs 1 and 2, we have used those obtained from the

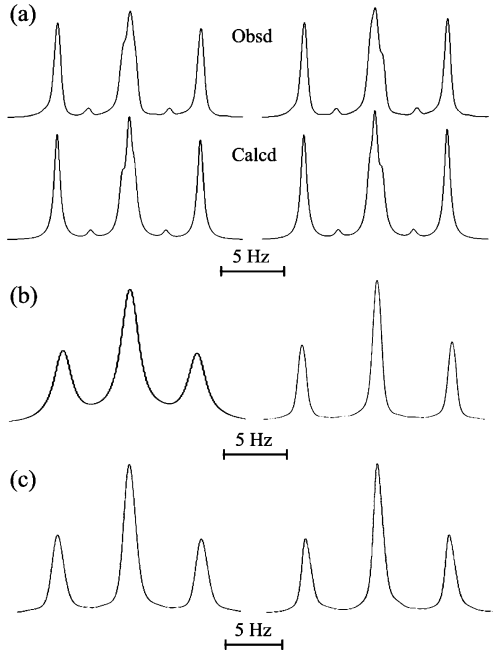

Figure 2. ^{1}H NMR spectra of methylene protons, A and A′ (left) and B and B′ (right), of MEMA dissolved in (a) D_2O at 25 °C, (b) $(CD_3)_2SO$ at 25 °C, and (c) MEDA dissolved in C_6D_{12} at 35 °C. For designations of the hydrogen atoms, see Figure 3b.

Table 1. Observed Vicinal ^{1}H−^{1}H and ^{13}C−^{1}H Coupling Constants of MEMA and MEDA[a]

		MEMA				MEDA			
	temp, °C	$^3J_{HH}$	$^3J'_{HH}$	$^3J^{CN}_{CH}$	$^3J^{CO}_{CH}$	$^3J_{HH}$	$^3J'_{HH}$	$^3J^{CN}_{CH}$	$^3J^{CO}_{CH}$
C_6D_{12}	15	6.52	3.63	3.45	2.90	5.91	5.91	4.72	3.23
	25	6.52	3.69	3.47	3.00	5.92	5.92	4.72	3.26
	35	6.51	3.78	3.48	3.02	5.92	5.92	4.76	3.34
	45	6.51	3.83	3.56	3.09	5.92	5.92	4.78	3.38
	55	6.48	3.92	3.66	3.16	5.97	5.97	4.79	3.43
$CDCl_3$ [b]	15	6.67	3.59	3.48	2.90				
	25	6.66	3.65	3.50	2.97				
	35	6.66	3.65	3.58	3.04				
	45	6.62	3.81	3.64	3.09				
	55	6.62	3.86	3.66	3.11				
$(CD_3)_2SO$ [c]	15	5.67	5.67			5.97	5.97	4.67	3.31
	25	5.69	5.69			5.97	5.97	4.66	3.37
	35	5.70	5.70			5.97	5.97	4.65	3.42
	45	5.71	5.71			5.97	5.97	4.67	3.48
	55	5.71	5.71			5.96	5.96	4.67	3.53
CD_3OD	15	6.63	3.98	3.54	2.97	5.60	5.60	4.47	3.00
	25	6.63	4.02	3.62	3.06	5.61	5.61	4.49	3.06
	35	6.62	4.09	3.66	3.08	5.63	5.63	4.51	3.10
	45	6.62	4.12	3.69	3.13	5.65	5.65	4.53	3.17
	55	6.59	4.18	3.82	3.16	5.68	5.68	4.53	3.20
D_2O	15	6.69	4.14	3.56	3.15	5.73	5.73	4.33	3.08
	25	6.66	4.24	3.62	3.22	5.76	5.76	4.38	3.16
	35	6.64	4.32	3.68	3.26	5.80	5.80	4.38	3.21
	45	6.60	4.45	3.80	3.31	5.84	5.84	4.41	3.26
	55	6.58	4.50	3.94	3.35	5.86	5.86	4.44	3.32

[a] In Hz. [b] MEDA is insoluble in chloroform. [c] ^{13}C NMR spectra of MEMA dissolved in $(CD_3)_2SO$ were too broad to give the coupling constants.

N−CH_2−CH_2−O bond sequence of 2MM. Figure 4 shows an example of observed and calculated ^{1}H NMR spectra of 2MM and its chemical structure. Listed in Table 2 are the vicinal coupling constants derived from the gNMR simulations. The p_t^{CC} and p_g^{CC} values were obtained from eqs 1 and 2 and divided by their sum to satisfy eq 3. The experimental p_t^{CC}

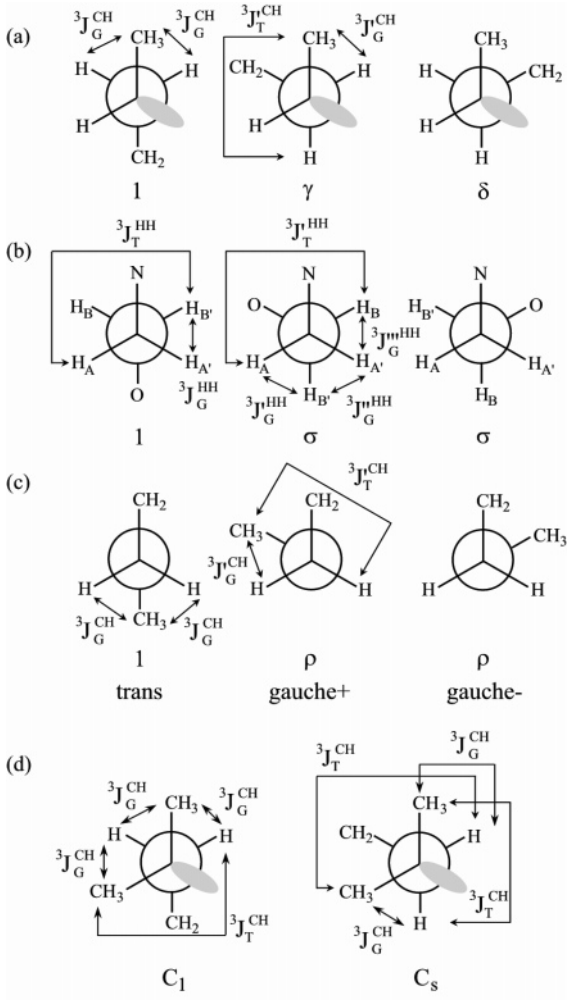

Figure 3. Conformations around the (a) NH−CH_2 (MEMA), (b) CH_2−CH_2 (MEMA and MEDA), (c) CH_2−O (MEMA and MEDA), and (d) N(CH_3)−CH_2 (MEDA) bonds with definitions of vicinal coupling constants. The Greek letters represent first-order interactions.

values are close to those obtained from the MO calculations (Table 3), except for those of the DMSO-d_6 solution,[30] which gave abnormally broad ^{13}C NMR spectra (Figure 5). This problem will be discussed later. The trans fraction increases with temperature or solvent polarity.

Figure 2c shows ^{1}H NMR spectra observed from MEDA dissolved in C_6D_{12}.[30] The vicinal coupling constants and trans fractions for MEDA are listed in Tables 1 and 3, respectively. Inasmuch as MEDA is insoluble in chloroform, the $CDCl_3$ parts of the two tables are blank. The experimental p_t^{CC} values agree well with the MO calculations, which were derived from the ΔG_k values (Table 4), as described previously.[4]

3.2. ^{13}C NMR. Figure 5 shows observed ^{13}C NMR spectra of methyl carbons of MEMA. The triplets are due to the vicinal couplings of $^{13}\underline{C}H_3$ −N−$C\underline{H}_2$ ($^3J^{CN}_{CH}$) or $^{13}\underline{C}H_3$−O−$C\underline{H}_2$ ($^3J^{CO}_{CH}$). The $^3J^{CX}_{CH}$ (X = N or O) values for the five solutions are listed in Table 1. The observed value is expressed as

$$^3J^{CX}_{CH} = {}^3J^{CH}_G\, p_t^{CX} + \frac{{}^3J'^{CH}_T + {}^3J'^{CH}_G}{2}\, p_g^{CX} \qquad (4)$$

where $^3J'^{CH}_T$ and $^3J^{CH}_G$'s are defined in Figure 3, and p_t^{CX} and p_g^{CX} are trans and gauche fractions of the C−X bond, respec-

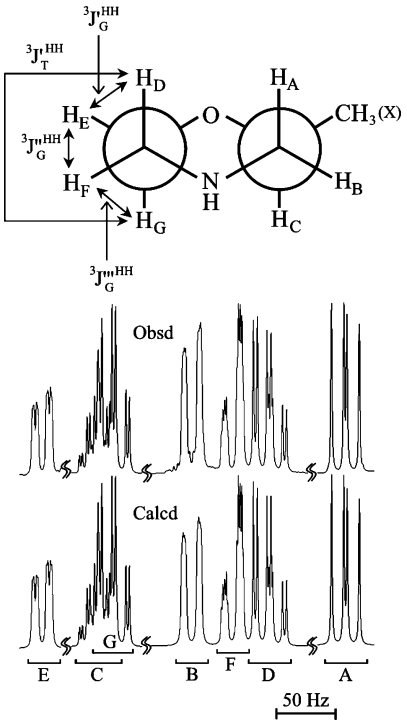

Figure 4. ^{1}H NMR spectra of 2-methylmorpholine (2MM) dissolved in D_2O at 25 °C. As shown, the peaks were assigned. The NMR parameters were determined as follows (δ relative to δ_{H_2O} in ppm and J in Hz): $\delta_A = 2.43$, $\delta_B = 2.86$, $\delta_C = 3.65$, $\delta_D = 2.73$, $\delta_E = 3.86$, $\delta_F = 2.79$, $\delta_G = 3.63$, $\delta_X = 1.11$, $^2J_{AB} = -12.90$, $^3J_{AC} = 10.20$, $^3J_{BC} = 2.41$, $^4J_{BF} = 1.25$, $^3J_{DE} = 3.46$, $^2J_{DF} = -13.03$, $^3J_{DG} = 11.92$, $^3J_{EF} = 1.29$, $^2J_{EG} = -11.71$, $^3J_{FG} = 2.54$, $^3J_{CX} = 6.31$.

Table 2. Vicinal ^{1}H−^{1}H Coupling Constants of 2MM[a]

solvent	$^3J'^{HH}_T$	$^3J'^{HH}_G$	$^3J''^{HH}_G$	$^3J'''^{HH}_G$	$^3J^{HH}_G$
C_6D_{12}	11.44	3.25	1.37	2.65	2.42
$CDCl_3$	11.62	3.33	1.21	2.51	2.35
$(CD_3)_2SO$	11.47	3.27	1.58	2.79	2.55
CD_3OD	11.71	3.48	1.33	2.58	2.46
D_2O	11.92	3.46	1.29	2.54	2.43

[a] In Hz. At 25 °C. For definitions of the coupling constants, see Figure 4. $^3J^{HH}_T = {}^3J'^{HH}_T$ and $^3J^{HH}_G = (^3J'^{HH}_G + {}^3J''^{HH}_G + {}^3J'''^{HH})/3$.

tively. For X = N, the $^3J^{CH}_G$, $^3J'^{CH}_T$, and $^3J'^{CH}_G$ values obtained from model compounds of PEI[4] have been used for the individual solutions: C_6D_{12}, $^3J'^{CH}_T = 7.80$ and $^3J^{CH}_G = {}^3J'^{CH}_G = 3.44$ Hz; $CDCl_3$, 7.62 and 3.41 Hz; $(CD_3)_2SO$, 7.23 and 3.52 Hz; CD_3OD, 7.41 and 3.28 Hz; D_2O, 7.52 and 3.05 Hz. For X = O, the $^3J^{CH}$ values optimized for 1,2-dimethoxyethane (DME) and PEO have been adopted for all the solutions: $^3J^{CH}_G = 2.0$ Hz and $^3J'^{CH}_T + {}^3J'^{CH}_G = 16.0$ Hz.[31] The p^{CX}_t values thus obtained are shown in Table 3. Both C−N and C−O bonds strongly prefer the trans state, and the trans fractions decrease as temperature or solvent polarity increases.

Figure 5c shows an example of ^{13}C NMR spectra of MEDA. The triplet and quasisextuplet stem from the $^{13}\underline{C}H_3-O-C\underline{H}_2$ and $^{13}\underline{C}H_3-N(CH_3)-C\underline{H}_2$ couplings, respectively. For MEDA, the $^3J^{CN}_{CH}$ value observed from the $^{13}\underline{C}H_3-N$ methyl carbon may be given by

$$^3J^{CN}_{CH} = \frac{^3J^{CH}_T + 3\,{}^3J^{CH}_G}{4} p^{CN}_{C_1} + \frac{^3J^{CH}_T + {}^3J^{CH}_G}{2} p^{CN}_{C_S} \qquad (5)$$

where $p^{CN}_{C_1}$ and $p^{CN}_{C_S}$ are fractions of C_1 and C_s forms around the C−N bond, respectively (see Figure 3): therefore, $p^{CN}_{C_1} + p^{CN}_{C_S} = 1$. Using the above-mentioned $^3J^{CH}$ values, we derived the $p^{CN}_{C_1}$ and p^{CO}_t values as shown in Table 3.

Table 3. Bond Conformations of MEMA and MEDA

			MEMA			MEDA		
medium	permittivity	temp, °C	p^{CN}_t	p^{CC}_t	p^{CO}_t	$p^{CN}_{C_1}$	p^{CC}_t	p^{CO}_t
			MO calcd					
gas phase	1.0	15	0.79	0.08	0.91	0.93	0.23	0.78
		25	0.78	0.08	0.90	0.92	0.24	0.77
		35	0.77	0.10	0.89	0.92	0.24	0.76
		45	0.75	0.10	0.88	0.91	0.24	0.75
		55	0.74	0.11	0.88	0.91	0.24	0.74
			NMR exptl					
C_6D_{12}	2.0	15	0.99	0.06	0.85	0.83	0.28	0.80
		25	0.99	0.06	0.83	0.83	0.28	0.79
		35	0.98	0.07	0.83	0.79	0.28	0.78
		45	0.95	0.08	0.82	0.77	0.28	0.77
		55	0.90	0.09	0.81	0.76	0.28	0.76
$CDCl_3$	4.8	15	0.97	0.05	0.85			
		25	0.96	0.06	0.84			
		35	0.92	0.06	0.83			
		45	0.89	0.07	0.82			
		55	0.88	0.07	0.82			
$(CD_3)_2SO$	46.7	15		0.28		0.76	0.28	0.78
		25		0.28		0.77	0.28	0.77
		35		0.28		0.78	0.28	0.76
		45		0.28		0.76	0.28	0.75
		55		0.28		0.76	0.28	0.75
CD_3OD	32.7	15	0.87	0.08	0.84	0.85	0.27	0.83
		25	0.84	0.08	0.82	0.83	0.27	0.82
		35	0.82	0.09	0.82	0.81	0.27	0.82
		45	0.80	0.09	0.81	0.79	0.27	0.81
		55	0.74	0.10	0.81	0.79	0.27	0.80
D_2O	78.5	15	0.77	0.10	0.81	0.86	0.28	0.82
		25	0.75	0.10	0.80	0.81	0.28	0.81
		35	0.72	0.11	0.79	0.81	0.28	0.80
		45	0.66	0.12	0.78	0.78	0.28	0.79
		55	0.60	0.13	0.78	0.76	0.28	0.78

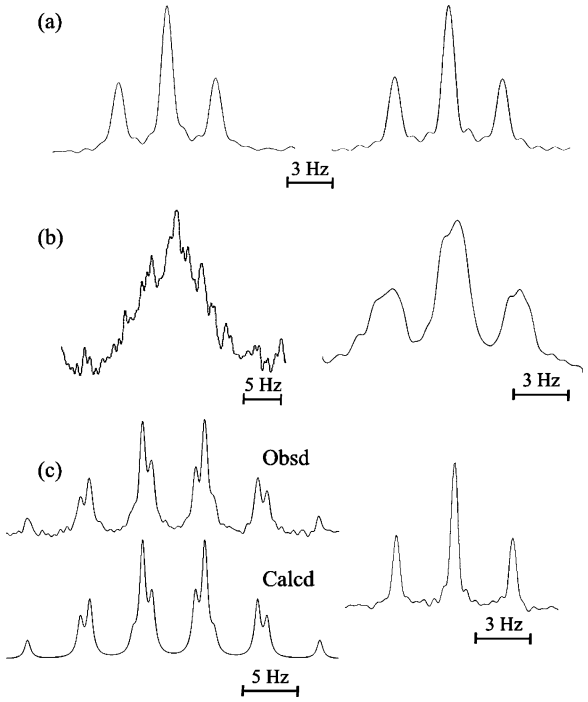

Figure 5. ^{13}C NMR spectra of methyl protons, $\underline{C}H_3N-$ (left) and $\underline{C}H_3O-$ (right), of (a) MEMA dissolved in D_2O at 25 °C, (b) in $(CD_3)_2\underline{S}O$ at 55 °C, and (c) MEDA dissolved in C_6D_{12} at 25 °C.

Table 4. Conformer Free Energies of MEMA and MEDA, Evaluated from Ab Initio MO Calculations

		l-MEMA		*l*-MEDA	
k	conformation	statistical weight[a]	ΔG_k[b] (kcal mol^{-1})	statistical weight[a]	ΔG_k[b] (kcal mol^{-1})
1	ttt	1	0.00	1	0.00
2	ttg$^+$	ρ	1.35	ρ	1.38
3	ttg$^-$	ρ	1.06	ρ	1.15
4	tg$^+$t	$\sigma\nu'$	1.01	$\sigma\nu'$	0.68
5	tg$^+$g$^+$	$\rho\sigma\nu'$	1.48	$\rho\sigma\nu'$	1.25
6	tg$^+$g$^-$	$\rho\sigma\nu'\omega'$	1.24	$\rho\sigma\nu'\omega'$	0.94
7	tg$^-$t	$\sigma\eta$	−1.76	$\sigma\omega$	−0.24
8	tg$^-$g$^+$	0		0	
9	tg$^-$g$^-$	$\rho\sigma\eta$	−0.35	$\rho\sigma\omega$	1.08
10	g$^+$tt	γ	1.05	γ	1.60
11	g$^+$tg$^+$	$\gamma\rho$	2.33	$\gamma\rho$	3.10
12	g$^+$tg$^-$	$\gamma\rho$	2.42	$\gamma\rho$	3.10
13	g$^+$g$^+$t	$\gamma\sigma\eta$	−0.77	$\gamma\sigma\omega$	0.92
14	g$^+$g$^+$g$^+$	$\gamma\rho\sigma\eta$	0.68	$\gamma\rho\sigma\omega$	2.29
15	g$^+$g$^+$g$^-$	0		0	
16	g$^+$g$^-$t	$\gamma\sigma\omega$	0.85	$\gamma\sigma\omega$	0.92
17	g$^+$g$^-$g$^+$	0		0	
18	g$^+$g$^-$g$^-$	$\gamma\rho\sigma\omega$	2.06	$\gamma\rho\sigma\omega$	2.29
19	g$^-$tt	δ	0.35	1	0.00
20	g$^-$tg$^+$	$\delta\rho$	1.57	ρ	1.15
21	g$^-$tg$^-$	$\delta\rho$	1.75	ρ	1.38
22	g$^-$g$^+$t	$\delta\sigma\omega$	0.21	$\sigma\omega$	−0.24
23	g$^-$g$^+$g$^+$	$\delta\rho\sigma\omega$	1.69	$\rho\sigma\omega$	1.08
24	g$^-$g$^+$g$^-$	0		0	
25	g$^-$g$^-$t	$\delta\sigma\nu'$	1.24	$\sigma\nu'$	0.68
26	g$^-$g$^-$g$^+$	$\delta\rho\sigma\nu'\omega'$	1.55	$\rho\sigma\nu'\omega'$	0.94
27	g$^-$g$^-$g$^-$	$\delta\rho\sigma\nu'$	2.14	$\rho\sigma\nu'$	1.25

[a] For the intramolecular interactions, see Figures 3, 7, and 8. [b] At the MP2/6-311++G(3df, 3pd)//HF/6-31G(d) level. Relative to the G_k value of the all-trans conformation. The blank indicates that the geometrical optimization did not detect the potential minimum; thus, the conformer is considered to be absent, and the null statistical weight is assigned thereto.

3.3. Association of MEMA with DMSO. The DMSO-d_6 solution gave broad ^{13}C NMR spectra (Figure 5b). The $\underline{C}H_3-O$ peaks can be considered a triplet, whereas the $\underline{C}H_3-NH$ signal loses the fine structure. In addition, the $C\underline{H}_2-NH$ protons exhibit a broader triplet than $C\underline{H}_2-O$ (Figure 2); that is, the former methylene group has a transverse relaxation time smaller than the latter. These facts suggest that the NH group may be anchored to a DMSO molecule. Accordingly, structures of the MEMA−DMSO complexes were searched for by MO calculations including the counterpoise correction[17,18] at the MP2/6-311+G(3df, 2p) level. As will be shown below, the C−C bond does not have its own conformational preference because of $E_\sigma \simeq 0$. The large gauche fraction of $p_g^{CC} \sim 0.80-0.95$ stems only from the hydrogen bonds. Therefore, two conformations, ttt and tgt, were initially set for MEMA and optimized together with a DMSO molecule. The resultant structures are depicted in Figure 6. The NBO analysis[19,20] for these two complexes evaluated the intermolecular N−H···O and C−H···O attractions as −2.40 and −1.89 kcal mol^{-1} (Figure 6a) and −6.20 and −1.21 kcal mol^{-1} (Figure 6b), respectively.[32] Because the N−H···O interactions are stronger than C−H···O's, the NH site may be more restricted in motion than the oxygen atom. This is consistent with the ^{1}H and ^{13}C NMR observations.

3.4. Conformational Energies of MEMA and MEDA. Statistical weight matrices, $\mathbf{U}_j$ (j: bond number), of MEMA and MEDA are given in the Appendix. The conformer free energies of the *l* forms, obtained from the MO calculations, are listed in Table 4, together with the statistical weights. Here, the *l* and *d* forms are defined according to the pseudoasymmetry of Flory[33,34] (see Figure 1). The first-, second-, and third-order interactions defined for MEMA (PEIEO) and MEDA (PMEIEO) are illustrated in Figures 3, 7, and 8. The statistical weights correspond to Boltzmann factors of the conformational energies: for example, $\sigma = \exp(-E_\sigma/RT)$, where R is the gas constant and T is the absolute temperature.[35,36] The conformational energies, determined by the least-squares method for the ΔG_k values as in previous studies,[2,4] are compared with those of PEI,[4] poly(trimethylene imine),[5] poly(*N*-methyltrimethylene imine),[5] PEO,[6] and their model compounds in Table 5.

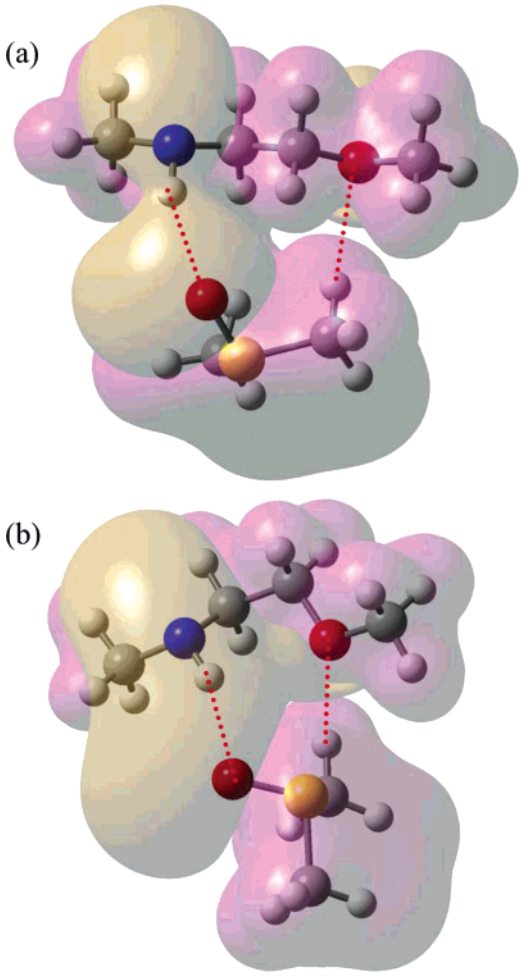

Figure 6. Molecular association of MEMA (a) in ttt and (b) tgt conformations with dimethyl sulfoxide.

Depending on whether the nitrogen site is secondary or tertiary, the first-order interaction energies can be grouped into two: secondary amine, MEMA, di-MEDA, and di-MPDA; tertiary amine, MEDA, and tetra-MPDA. Each group seems to have its own energy set. The E_σ values are nearly null except for that of DME; the C−C bonds do not possess their intrinsic conformational preferences.

Three types of hydrogen bonds were found in MEMA: η, N−H···O; ω, C−H···O; ω', C−H···N. Of these, the η attraction is the strongest ($E_\eta = -1.75$ kcal mol^{-1}) and surpasses the N−H···N hydrogen bond (−1.54 kcal mol^{-1}) of di-MEDA (PEI).[4] In contrast, MEDA has only weak C−H···O (ω) and C−H···N (ω') attractions because its nitrogen site has no hydrogen atom. Both MEMA and MEDA form C−H···O hydrogen bonds, which are, however, much weaker than that of DME (PEO).[6]

3.5. Configurational Properties of PEIEO and PMEIEO. According to the IRIS scheme,[4,5] the *meso*-diad probabilities (P_m's) and unperturbed characteristic ratios ($\langle r^2\rangle_0/nl^2$'s) of PEIEO and PMEIEO were calculated from the conformational energies

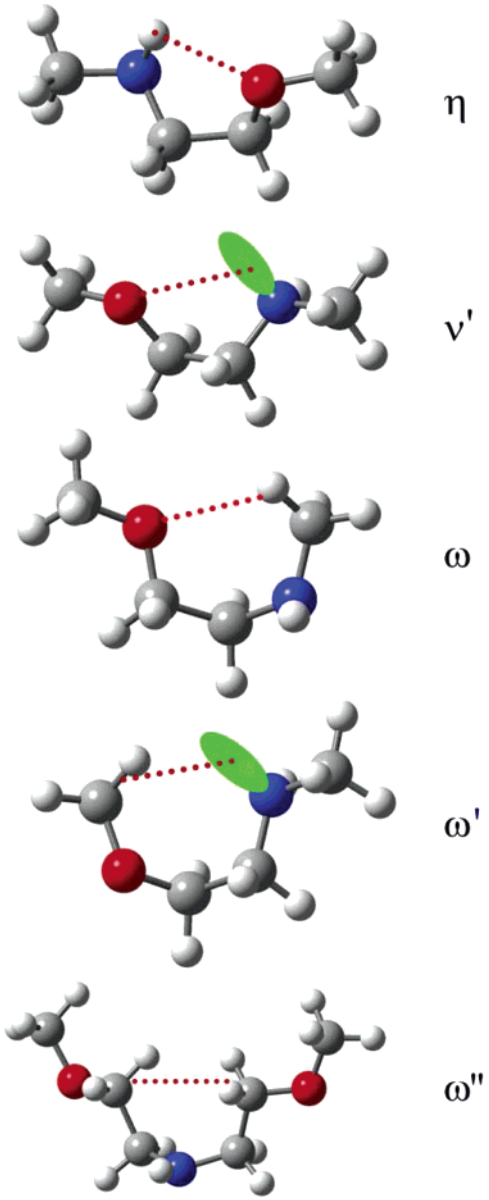

Figure 7. Second- and third-order intramolecular interactions defined for MEMA and PEIEO.

given in Table 5 and statistical weight matrices in Appendix. The combined statistical weight matrix W_i of the ith repeating unit (eq 16 of ref 5) is defined as

$$W_i = \begin{pmatrix} V_i^{ll} & V_i^{ld} \\ V_i^{dl} & V_i^{dd} \end{pmatrix} \tag{6}$$

where, for example, V_i^{ld} ($i \geq 2$) is calculated from

$$V_i^{ld} = \mathbf{U}_a^l \mathbf{U}_b^l \mathbf{U}_c^l \mathbf{U}_d^l \mathbf{U}_e^l \mathbf{U}_f^d \tag{7}$$

Here, the configuration ld represents that the ith and $(i + 1)$th repeating units adopt the l and d forms, respectively. The other V_i^α ($\alpha = ll, dd, dl$) matrices are also expressed as products of the statistical weight matrices (see Table 6). From the W_i matrices, the P_m values of PEIEO and PMEIEO were calculated to be 0.50. Inasmuch as six bonds separate the neighboring nitrogen sites, the stereochemical correlation between them is hardly retained, and these copolymers behave as atactic chains. The characteristic ratios were calculated for the n_c chains

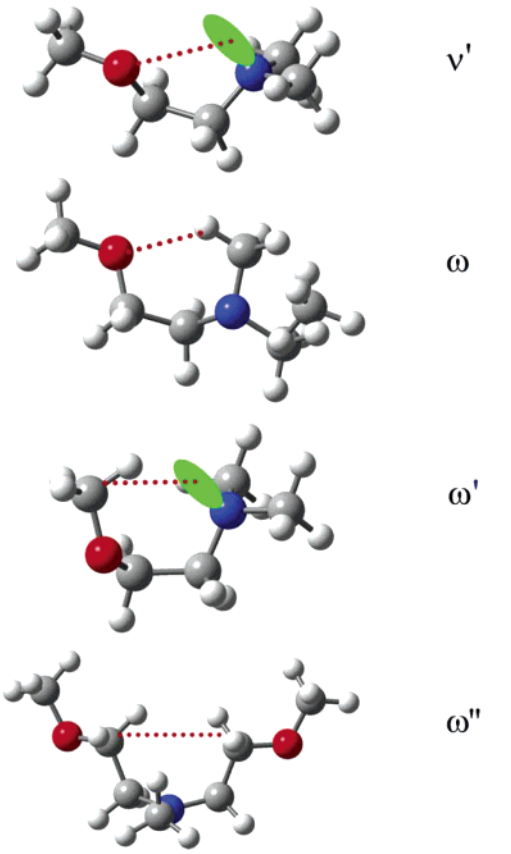

Figure 8. Second- and third-order intramolecular interactions defined for MEDA and PMEIEO.

Table 5. Conformational Energies (kcal mol^{-1}) of MEMA (PEIEO), MEDA (PMEIEO), Di-MEDA (PEI), Di-MPDA (PTMI), Tetra-MPDA (PMTMI), and DME (PEO), Derived from Ab Initio MO Calculations[a]

	MEMA (PEIEO)	MEDA (PMEIEO)	di-MEDA (PEI)	di-MPDA (PTMI)	tetra-MPDA (PMTMI)	DME (PEO)
			First-Order Interaction			
E_γ	1.06	1.52	1.06	1.16	1.41	
E_δ	0.44		0.54	0.53		
E_σ	0.05	0.03	−0.09	−0.06	−0.11	0.32
E_ρ	1.21	1.27				1.22
			Second- and Third-Order Interactions			
E_η	−1.75		−1.54			
E_ν			−0.58			
$E_{\nu'}$	0.59	0.30	1.16			
E_ω	−0.21	−0.41	0.97			−1.12
$E_{\omega'}$	−0.68	−0.66	0.61			
$E_{\omega''}$[b]	1.24	0.41	0.94			

[a] Abbreviations: MEMA, *N*-(2-methoxyethyl)methylamine; PEIEO, poly(ethylene imine-*alt*-ethylene oxide); MEDA, *N*,*N*-(2-methoxyethyl)dimethylamine; PMEIEO, poly(*N*-methylethylene imine-*alt*-ethylene oxide); di-MEDA, *N*,*N*′-dimethylethylenediamine; PEI, poly(ethylene imine); di-MPDA, *N*,*N*′-dimethyl-1,3-propanediamine; PTMI, poly(trimethylene imine); tetra-MPDA, *N*,*N*,*N*′,*N*′-tetramethyl-1,3-propanediamine; PMTMI, poly(*N*-methyltrimethylene imine); DME, 1,2-dimethoxyethane; PEO, poly(ethylene oxide). For definitions of the interactions, see Figures 3, 7, and 8. Conformational energies of di-MEDA, di-MPDA, tetra-MPDA, and DME are compared with those for the analogous interactions of MEMA and MEDA. [b] Evaluated from dimeric model compounds (see Figures 7 and 8).

generated so as to satisfy $P_m = 0.50$ and averaged to yield the mean $\langle r^2 \rangle_0 / nl^2$ value. In the calculations, the dihedral angles were chosen for the individual diads as shown in Tables 6 and 7. The bond lengths and bond angles are also given in Table 7.

Table 6. Statistical Weight Matrices and Dihedral Angles Used in IRIS Calculations for Individual Configurations

configuration[a]	statistical weight matrix[b]						dihedral angle[b]					
ll	$\mathbf{U}_a^l$	$\mathbf{U}_b^l$	$\mathbf{U}_c^l$	$\mathbf{U}_d^l$	$\mathbf{U}_e^l$	$\mathbf{U}_f^l$	ϕ_a^l	ϕ_b^l	ϕ_c^l	ϕ_d^l	ϕ_e^l	ϕ_f^l
dd	$\mathbf{U}_a^d$	$\mathbf{U}_b^d$	$\mathbf{U}_c^d$	$\mathbf{U}_d^d$	$\mathbf{U}_e^d$	$\mathbf{U}_f^d$	ϕ_a^d	ϕ_b^d	ϕ_c^d	ϕ_d^d	ϕ_e^d	ϕ_f^d
ld	$\mathbf{U}_a^l$	$\mathbf{U}_b^l$	$\mathbf{U}_c^l$	$\mathbf{U}_d^l$	$\mathbf{U}_e^l$	$\mathbf{U}_f^d$	ϕ_a^l	ϕ_b^l	ϕ_c^l	ϕ_d^d	ϕ_e^d	ϕ_f^d
dl	$\mathbf{U}_a^d$	$\mathbf{U}_b^d$	$\mathbf{U}_c^d$	$\mathbf{U}_d^d$	$\mathbf{U}_e^d$	$\mathbf{U}_f^l$	ϕ_a^d	ϕ_b^d	ϕ_c^d	ϕ_d^l	ϕ_e^l	ϕ_f^l

[a] For example, *ld* represents that the *i*th, and $(i + 1)$th repeating units adopt the *l* and *d* forms, respectively. [b] In the *i*th monomeric unit. For example, $\mathbf{U}_a^l$ and ϕ_a^l represent the statistical weight matrix and dihedral angle of bond a in the *l* form, respectively. For the first monomeric unit, the $\mathbf{U}_2-\mathbf{U}_7$ matrices and $\phi_2-\phi_7$ angles are chosen similarly.

Table 7. Geometrical Parameters Used in IRIS Calculations for PEIEO and PMEIEO[a]

			dihedral angle (ϕ), deg					
			PEIEO			PMEIEO		
configuration	bond		t	g^+	g^-	t	g^+	g^-
l form	2	a	−6.7	112.8	−94.7	−25.4	112.9	−101.0
	3	b	0.0	111.2	−116.1	0.0	110.0	−99.5
	4	c	0.0	92.6	−96.7	0.0	90.7	−93.4
	5	d	0.0	96.7	−92.6	0.0	93.4	−90.7
	6	e	0.0	116.1	−111.2	0.0	99.5	−110.0
	7	f	6.7	94.7	−112.8	25.4	101.0	−112.9
d form	2	a	6.7	94.7	−112.8	25.4	101.0	−112.9
	3	b	0.0	116.1	−111.2	0.0	99.5	−110.0
	4	c	0.0	96.7	−92.6	0.0	93.4	−90.7
	5	d	0.0	92.6	−96.7	0.0	90.7	−93.4
	6	e	0.0	111.2	−116.1	0.0	110.0	−99.5
	7	f	−6.7	112.8	−94.7	−25.4	112.9	−101.0

[a] Obtained by the geometrical optimization for MEMA and MEDA at the HF/6-31G(d) level. Bond lengths and bond angles for PEIEO (PMEIEO) are as follows: $l_{CN} = 1.45$ (1.45) Å, $l_{CC} = 1.52$ (1.52) Å, $l_{CO} = 1.39$ (1.40) Å, ∠CNC = 113.8 (112.3)°, ∠NCC = 110.3 (112.3)°, ∠CCO = 108.3 (107.6)°, and ∠COC = 114.3 (114.3)°. The dihedral angles, depending on the conformer, fluctuate within ± 10°. The fluctuation yields a 7% margin of the calculated $\langle r^2\rangle_0/nl^2$ value.

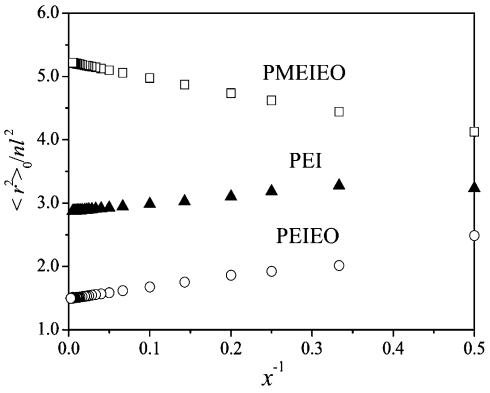

Figure 9. Characteristic ratios of PEIEO, PMEIEO, and PEI ensembles of $n_c = 512$ as a function of the reciprocal (x^{-1}) of degree of polymerization. The extrapolation to $x^{-1} = 0$ gives the $\langle r^2\rangle_0/nl^2$ value for the infinite chain ($x \to \infty$).

In Figure 9, the characteristic ratios of PEIEO and PMEIEO ensembles of $n_c = 512$ are plotted against the reciprocal degree of polymerization, x^{-1}. For comparison, the data on PEI[4] ($n_c = 512$) are also plotted. The characteristic ratios were calculated from the conformational energies shown in Table 5, thus representing the isolate chain in vacuo and in nonpolar solvents. The $\langle r^2\rangle_0/nl^2$ values at $x^{-1} = 0$ (infinite chain) are 1.5 (PEIEO), 5.2 (PMEIEO), and 2.9 (PEI). The $\langle r^2\rangle_0/nl^2$ value of PEIEO decreases with increasing *x*, and that of PEI exhibits a maximum around $x^{-1} = 0.33$ and decreases toward $x^{-1} = 0$. As seen for PMEIEO, most polymers show monotonic increases in $\langle r^2\rangle_0/nl^2$ with *x*; therefore, the behaviors of PEIEO and PEI are exceptional. So far, an analogous $\langle r^2\rangle_0/nl^2$ vs x^{-1} curve has been found for syndiotactic poly(methyl methacrylate) and ascribed to quasicyclic paths formed in the main chain.[37] Recently, Mattice et al.[38] have derived the following relation:

$$\left(\frac{\mathrm{d}\langle r^2\rangle_0/nl^2}{\mathrm{d}x^{-1}}\right)_{x^{-1}=0} = -2\sum_{k=1}^{\infty} k\langle \mathbf{u}_j\cdot\mathbf{u}_{j+k}\rangle_0 \qquad (8)$$

where the subscript 0 indicates the unperturbed state, and $\mathbf{u}_j$ is the unit vector along the *j*th bond. According to eq 8, the positive $(\mathrm{d}\langle r^2\rangle_0/nl^2/\mathrm{d}x^{-1})_{x^{-1}=0}$ values of PEIEO and PEI stem from negative $k\langle \mathbf{u}_j\cdot\mathbf{u}_{j+k}\rangle_0$ terms.

3.6. Orientation Correlation between Bonds. The scalar product between unit vectors, $\mathbf{u}_j$ and $\mathbf{u}_{j+k}$, along the *j*th and $(j + k)$th bonds can be averaged over all possible conformations of bonds in the repeating unit (n_1 = a−f and $n_b = 6$ for PEIEO and PMEIEO; n_1 = a−c and $n_b = 3$ for PEI, see Figure 1) and all configurations of the n_c chains in the ensemble according to

$$\overline{\langle \mathbf{u}_j\cdot\mathbf{u}_{j+k}\rangle_0} = \frac{1}{n_b\, n_c}\sum_{n_1=\mathrm{a}}^{\mathrm{f\ or\ c}}\sum_{n_2=1}^{n_c}\langle T_jT_{j+1}\cdots T_{j+k-1}\rangle_{11}^{n_1,n_2} \qquad (9)$$

where the overbar stands for the average for the bond and configuration, the angular brackets represent the average for the conformation, and $\langle T_jT_{j+1}\cdots T_{j+k-1}\rangle_{11}^{n_1,n_2}$ corresponds to the (1, 1) element of $\langle T_jT_{j+1}\cdots T_{j+k-1}\rangle^{n_1,n_2}$ calculated from[35,36,38]

$$\langle T_jT_{j+1}\cdots T_{j+k-1}\rangle^{n_1,n_2} = z_{n_2}^{-1}[(J^*\mathbf{U}_1\cdots\mathbf{U}_{j-1})\otimes E_3]\times [(\mathbf{U}_j\otimes E_3)||T_j||\cdots(\mathbf{U}_{j+k-1}\otimes E_3)||T_{j+k-1}||][(\mathbf{U}_{j+k}\cdots\mathbf{U}_n)\otimes E_3] \qquad (10)$$

Here, T_j is the transformation matrix from the *j*th to $(j - 1)$th frame of reference, ⊗ stands for direct product, and E_3 is the identity matrix of size 3. The partition function of the n_2th chain, z_{n_2}, is given by

$$z_{n_2} = J^*(\prod_{j=2}^{n-1}\mathbf{U}_j)J \qquad (11)$$

where $J^* = [100]$, $\mathbf{U}_j$'s are the **U** matrices chosen in accordance with the configurational sequence of the n_2th chain, and *J* is the column matrix whose elements are unity. In general, $\overline{\langle \mathbf{u}_j\cdot\mathbf{u}_{j+k}\rangle_0}$ decreases rapidly with increasing *k*; therefore, an amplification factor *k* has been introduced to detect up to the long-range correlation. Because $\mathbf{u}_j\cdot\mathbf{u}_{j+k} = \cos\theta_{j,j+k}$ ($\theta_{j,j+k}$: angle between $\mathbf{u}_j$ and $\mathbf{u}_{j+k}$), the $k\overline{\langle \mathbf{u}_j\cdot\mathbf{u}_{j+k}\rangle_0}$ term can also be expressed as

$$k\overline{\langle \mathbf{u}_j\cdot\mathbf{u}_{j+k}\rangle_0} = k\overline{\langle\cos\theta_{j,j+k}\rangle_0} \qquad (12)$$

Accordingly, the $k\overline{\langle \mathbf{u}_j\cdot\mathbf{u}_{j+k}\rangle_0}$ term quantifies the orientation correlation between bonds *j* and $j + k$. Figure 10 shows $k\overline{\langle \mathbf{u}_j\cdot\mathbf{u}_{j+k}\rangle_0}$ vs *k* curves of PEIEO, PMEIEO, and PEI. The percentage indicates the hydrogen bond strength (HBS in %);[4] in the calculations, the hydrogen bond energies were adjusted with $E_\xi \times$ HBS (%)/100, where E_ξ's are the interaction energies ($\xi = \eta$, ω, and ω' for PEIEO, ω and ω' for PMEIEO, and η and ν for PEI[4]) as obtained from the MO calculations (Table 5). The other energy parameters were set as in Table 5.

When HBS = 100%, PEIEO gives negative $k\overline{\langle \mathbf{u}_j\cdot\mathbf{u}_{j+k}\rangle_0}$ values for $6 \le k \le 15$ and the minimum at $k = 9$. The curve includes two periodic variations: an odd−even oscillation and an intense long-period undulation. The latter diminishes with

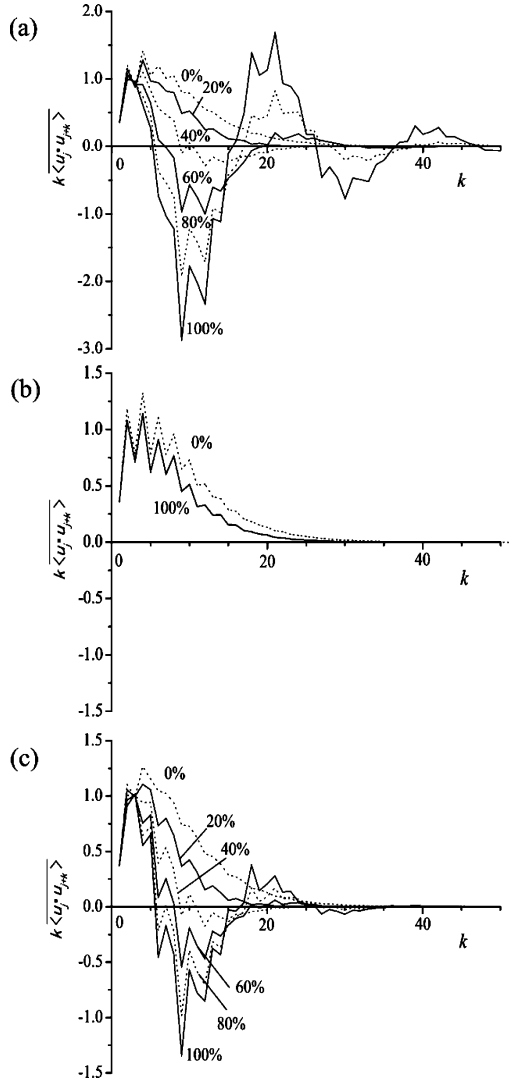

Figure 10. $k\overline{\langle \mathbf{u}_j \cdot \mathbf{u}_{j+k} \rangle_0}$ vs k curves of (a) PEIEO, (b) PMEIEO, and (c) PEI. The percentage represents the hydrogen bond strength (HBS).

an increase in HBS and disappears around HBS = 20%, but the former appears independently of HBS; accordingly, the long-range undulation may be ascribed to the hydrogen bonds. Although PEI shows analogous curves, the minima are about half of those for PEIEO. This is because PEIEO forms stronger hydrogen bonds than PEI. In contrast, PMEIEO shows only the odd−even oscillation; its hydrogen bonds are so weak that the curve shows only a slight change between HBS = 100 and 0%. If the hydrogen bonds were completely ineffective (HBS = 0%), the three polymers would give similar curves.

Figure 11 illustrates examples of especially stable conformations: (a) $(tg^-ttg^+t)_2$ of PEIEO; (b) $(tg^+ttg^-t)_2$ of PEI. Then, the successive hydrogen bonds are formed to stabilize the circular paths by $4E_\sigma + 4E_\eta$ (−6.8 (PEIEO) and −6.52 (PEI) kcal mol^{-1}) as compared with the all-trans state. The $\mathbf{u}_j$ vector seems to form an angle larger than $\pi/2$ with $\mathbf{u}_{j+6}$ and run antiparallel to $\mathbf{u}_{j+9}$; therefore, the $k\overline{\langle \mathbf{u}_j \cdot \mathbf{u}_{j+k} \rangle_0}$ term turns negative at $k = 6$ ($\cos \theta_{j,j+6} < 0$) and shows the minimum at $k = 9$ ($\cos \theta_{j,j+9} \sim -1$). These relationships are consistent with the orientation correlations of PEIEO and PEI in Figure 10 and valid even if the $\mathbf{u}_j$ vector is set to any bond in the circular path. The $k\overline{\langle \mathbf{u}_j \cdot \mathbf{u}_{j+k} \rangle_0}$ vs k curves, obtained from all the conformations, strongly reflect low-energy states, e.g., those shown in Figure 11. Such circular paths may be frequently formed in PEIEO and PEI chains. The $\langle r^2 \rangle_0 / nl^2$ value of PEIEO of HBS = 100% is as small as 1.5, being close to that (1.0) of the freely jointed chain.[35,36] However, the PEIEO chain is exceedingly subject to the intramolecular hydrogen bonds and hence far from flexible. As the hydrogen bonds are relaxed, the PEIEO chain will expand considerably: $\langle r^2 \rangle_0 / nl^2$ = 1.5 (HBS = 100%), 2.2 (80%), 3.2 (60%), 4.5 (40%), 5.7 (20%), 6.5 (0%). The PEI chain behaves similarly: $\langle r^2 \rangle_0 / nl^2$ = 2.9 (HBS = 100%), 3.3 (80%), 3.8 (60%), 4.5 (40%), 5.4 (20%), 6.3 (0%). On the other hand, PMEIEO shows only a slight change: $\langle r^2 \rangle_0 / nl^2$ = 5.2 (HBS = 100%), 5.9 (0%).

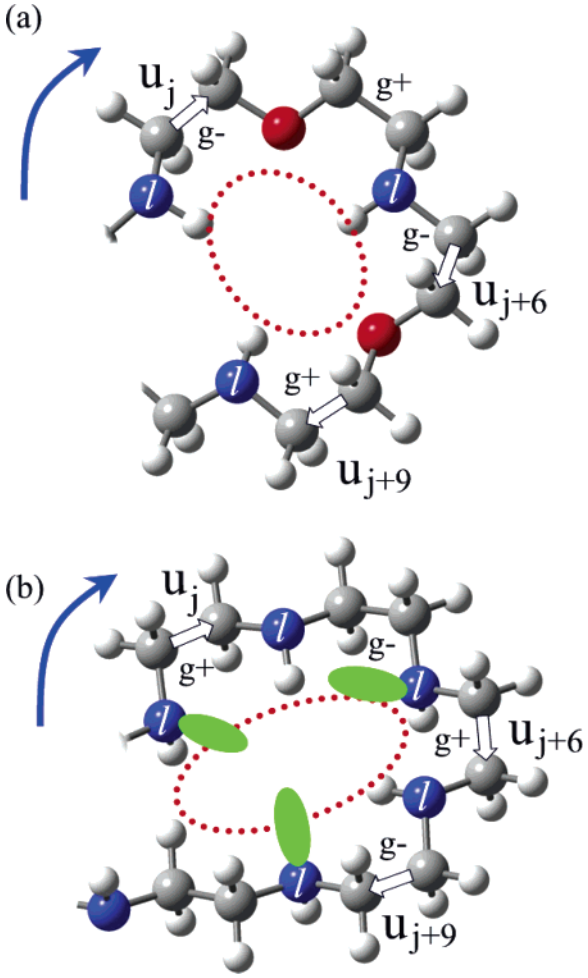

Figure 11. Examples of circular paths stabilized by successive hydrogen bonds: (a) $(tg^-ttg^+t)_2$ of PEIEO, (b) $(tg^+ttg^-t)_2$ of PEI.

3.7. Crystal Structure of PEIEO. Even in the crystalline state, most polymers will keep their most stable conformations.[2] As stated above, the C−N and C−O bonds of PEIEO have strong trans preferences (E_γ = 1.06 and E_ρ = 1.21 kcal mol^{-1}), whereas the C−C bond would be flexible without the intramolecular hydrogen bonds because $|E_\sigma|$ is as small as 0.05 kcal mol^{-1}. The N−C−C−O bonds of PEIEO must adopt either the ttt or the tgt state in the crystal. Most of all-trans polyethers without bulky substituents are expected to be packed in either an orthorhombic polyethylene-type[39,40] or a monoclinic poly(tetramethylene oxide)-type[41] lattice. The former lattice includes two chains whose molecular planes intersect each other roughly perpendicularly. In the latter lattice, two all-trans chains are parallel to each other probably because of electrostatic and dipole−dipole interactions. When the all-trans chains are arranged, the following conditions may be fulfilled: (1) to avoid lone pair−lone pair repulsions, (2) to cancel out dipole moments

along bisectors of the C−O−C and C−N−C angles, and (3) to form intermolecular N−H···O and N−H···N hydrogen bonds. For PEIEO, however, we could not find any molecular packings to satisfy all the requisites. Accordingly, all-trans deca(ethylene imine-*alt*-ethylene oxide)s were packed in some kinds of single crystals composed of 10 × 10 orthorhombic or monoclinic lattices so as to partly satisfy the above conditions and underwent the geometrical optimization using the Sander module of the Amber8 program.[23] In every case, however, the optimized structure had comparatively large vacancies between the molecular chains and the N−H···O and N−H···N distances were much larger than the sums of the van der Waals radii. The crystal of all-trans PEIEO chains would be improbable.

Poly(ethylene oxide) crystallizes to adopt the tgt conformation in the O−C−C−O bond sequence;[42,43] the all-trans state has also been found only in the stretched samples,[44,45] thus being metastable. In a dry environment, a pair of PEI chains take the tgt conformation in the N−C−C−N bonds to form a double helix,[46] which is supported by intermolecular N−H···N hydrogen bonds. Next, we set two deca(ethylene imine-*alt*-ethylene oxide)s in the double-stranded helix with the same one-dimensional periodicity as that of anhydrous PEI so that intramolecular and intermolecular hydrogen bonds would be formed effectively, and the geometry was optimized with the Sander module. The resultant structure is shown in Figure 12a, and the geometrical parameters are listed in Table 8. The hydrogen bond distances were optimized as 2.45 Å (intramolecular N−H···O), 2.73 Å (intermolecular N−H···O), and 2.23 Å (intermolecular N−H···N).

The double helix was further optimized by MO calculations at the B3LYP/6-31G(d) level under the one-dimensional periodic boundary condition.[21,22] The optimum structure and geometrical parameters are compared with those by Amber8 in Figure 12b and Table 8, respectively; noticeable differences between the Amber and MO calculations can be found in ϕ_{CC} and ϕ_{CO}. The hydrogen bond distances are 2.62 Å (intramolecular N−H···O), 2.62 Å (intermolecular N−H···O), and 2.26 Å (intermolecular N−H···N). By the NBO analysis[19,20] using the 6-31G(d) basis set, the intermolecular hydrogen bond energies were estimated as −0.95 kcal mol^{-1} (N−H···O) and −7.42 kcal mol^{-1} (N−H···N), respectively.[32,47] The shorter N−H···N hydrogen bond is suggested to be much stronger than N−H···O. The PEIEO chain adopts tg$^+$ttg$^+$t conformation in the N (*l* form)−C−C−O−C−C−N (*l* form) bond sequence. The corresponding statistical weight is $\sigma^2\eta\nu'$; therefore, the intermolecular energy, including the intramolecular N−H···O energy (E_η), can be calculated as $2E_\sigma + E_\eta + E_{\nu'} = -1.06$ kcal mol^{-1}. Only from the above interactions, the helical chain is suggested to be stabilized by as much as $-1.06 - 0.95 - 7.42 = -9.43$ kcal mol^{-1} per repeating unit as compared with the isolated all-trans chain.

From the above results, it seems reasonable to anticipate that crystallized PEIEO forms the double-helical structure of the tgt conformation. In contrast with PEI, which is apt to capture water molecules and render itself all-trans,[48,49] PEIEO may be little affected by water because no particularly large differences in p_t's of MEMA can be found between the C_6D_{12} and aqueous solutions (Table 3). The double helix of PEIEO is expected to be stable even in high humidity. In the melt and solutions, the stable circular paths (Figure 11) may frequently occur. Therefore, careful crystallization should be required; otherwise, only amorphous solids would be yielded.

3.8. Expected Properties and Suggestions for the Synthesis. The pH value of the monomeric model compound of PEI, *N*,*N*′-dimethylethylenediamine, is 9.9,[50] close to that (∼10) of PEI.[51] From the p*K*a value (8.96) of MEDA,[52] PMEIEO and PEIEO are expected not to be so basic and cytotoxic as PEI. As the NMR experiments show that p_t^{CC} of MEMA is almost independent of solvent, even protic solvents such as methanol and water can hardly break the intramolecular N−H···O hydrogen bond; therefore, pure water may be a poor solvent for PEIEO. In vivo, however, the pH value is so adjusted as to be neutral, and hence PEIEO and PMEIEO will be protonated and soluble. Comparison between PEIEO and PMEIEO shows that replacement of the NH hydrogen with a bulky substituent renders the main chain flexible and readily soluble.

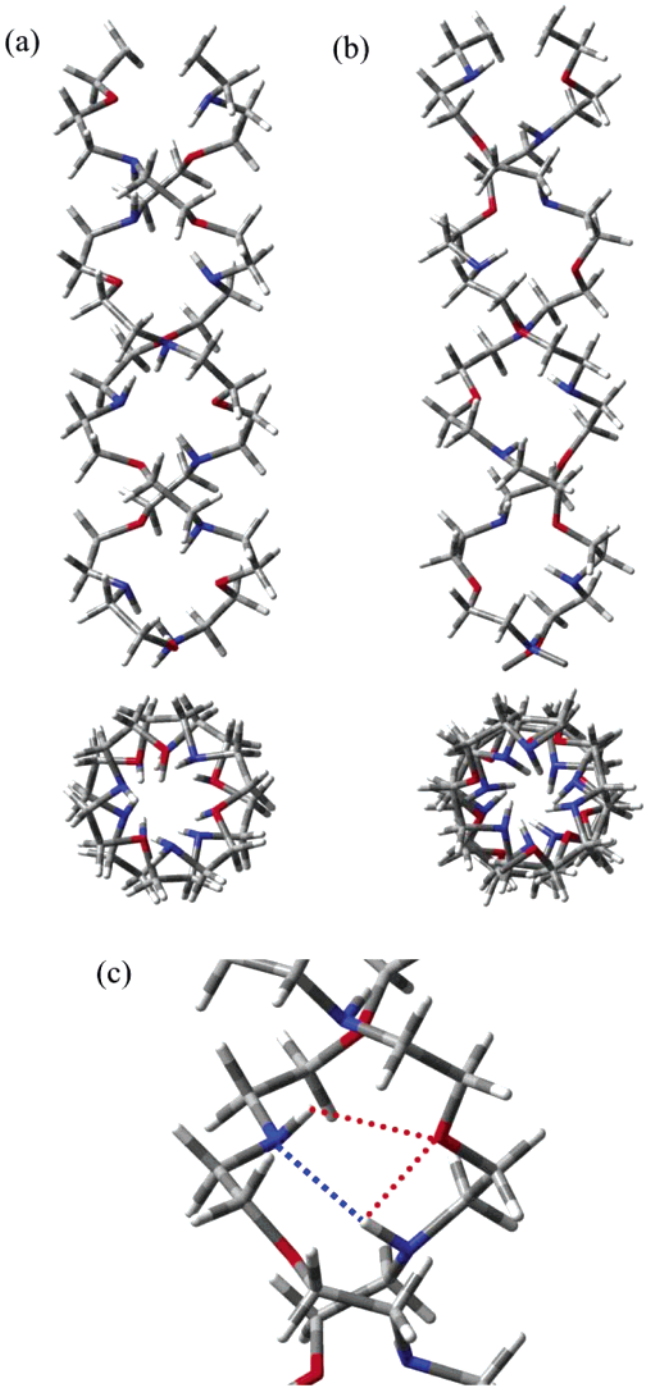

Figure 12. Double-stranded helices of PEIEO, optimized by (a) Amber and (b) MO calculations at the B3LYP/6-31G(d) level under the periodic boundary condition. (c) Intramolecular N−H···O, intermolecular N−H···O, and intermolecular N−H···N hydrogen bonds.

Table 8. Optimized Geometrical Parameters of Double-Stranded Helix of PEIEO

bond length, Å		
	amber	B3LYP/6-31G(d)
l_{CN}	1.48	1.46
l_{CC}	1.53	1.52
l_{CO}	1.42	1.42
bond angle, deg		
	amber	B3LYP/6-31G(d)
∠CNC	110.7	111.3
∠NCC	112.8	113.1
∠CCO	111.0	110.5
∠COC	112.5	113.7
dihedral angle, deg		
	amber	B3LYP/6-31G(d)
ϕ_{NC}	7.1	9.8
ϕ_{CC}	132.3	119.0
ϕ_{CO}	11.0	21.8
fiber period, Å		
	amber	B3LYP/6-31G(d)
	19.34	21.43
hydrogen bond distance, Å		
	amber	B3LYP/6-31G(d)
intramolecular N−H···O	2.45	2.62
intermolecular N−H···O	2.73	2.62
intermolecular N−H···N	2.23	2.26

If PEIEO is used as a polymer electrolyte, the added metallic ion, e.g., Li^+, would break the intramolecular hydrogen bonds and Li^+···NH and Li^+···O attractions would be formed. If one desires to enhance the ion conductivity of the polymer matrix, one should partly replace the NH hydrogen atoms with, e.g., methyl or longer alkyl groups. The substituents moderately disturb the Li^+···O and Li^+···N interactions, expand the polymer matrix, and increase the free volume. Consequently, a higher ion conductivity would be observed from the partially substituted PEIEO. For example, methylation of PEIEO will be feasible with formalin and formic acid.[53] The properties and functions of PEIEO may be adjusted by the degree of alkylation.

As mentioned in the Introduction, oligo(ethylene imine-*alt*-ethylene oxide) was synthesized by homopolymerization of *N*-(2-hydroxyethyl)aziridine in a mixed solvent of CCl_4 and SO_2 at −15 °C.[14] As discussed in Section 3.3, MEMA associates with DMSO. Similarly, the oligomer forms a complex with SO_2. As soon as the polymerization starts, the product must be bound by the intramolecular hydrogen bond, shrunk, and precipitated. A good solution for this problem is to introduce a blocking group onto the nitrogen atom. A long and flexible substituent not only prevents the hydrogen bonds but also generates the configurational entropy by itself to enhance the solubility. After the polymerization, one may remove the protecting group. Fortunately, ring-opening polymerizations of unsubstituted[54] and 2-substituted[53] 2-oxazolines for PEI and 2-substituted 5,6-dihydro-4*H*-1,3-oxazines for poly(trimethylene imine)[55] satisfy the essential requisite.

4. Concluding Remarks

As shown above, we have elucidated conformational characteristics of PEIEO and PMEIEO and the secondary structure of the circular path of PEIEO by the IRIS analysis of ab initio MO calculations and NMR experiments for the model compounds, predicted the crystal structure of PEIEO by the molecular mechanics computations and the density functional MO calculations under the periodic boundary condition, discussed their functions and applications, and proffered advice on the synthesis. In conclusion, these alternating copolymers are worth synthesizing and characterizing, and this study has shown the possibility of molecular design for new polymers by means of computational chemistry and supporting experiments.

Conformational characteristics, higher-order structures, physical properties, and functions of polymers including nitrogen and oxygen, e.g., PEO, PEI, and PEIEO, are essentially determined by the attractive interactions due to the heteroatoms. For PEO, a variety of Θ conditions and a wide range (4.1−9.7) of unperturbed characteristic ratios have been reported.[6] This may be partly due to experimental errors or incorrect Θ conditions but can also be explained as follows. The concept of the Θ state is based on the Flory−Huggins theory[56] of polymer solutions. The interaction-energy change due to mixing of polymer and solvent is assumed as

$$\Delta w_{12} = w_{12} - \frac{1}{2}(w_{11} + w_{22}) \tag{13}$$

where w represents the interaction energy, and the subscripts 11, 12, and 22 stand for solvent−solvent, solvent−polymer, and polymer−polymer combinations, respectively. The so-called χ parameter is defined as

$$\chi = \frac{z\Delta w_{12}}{kT} \tag{14}$$

where z is the coordination number and k is the Boltzmann constant. The interaction-energy change may also be expressed as a function,

$$\Delta w_{12} = f(\Delta\alpha_1, \Delta\alpha_2, \Delta\alpha_3, ..., \Delta\beta_1, \Delta\beta_2, \Delta\beta_3, ...) \tag{15}$$

where $\Delta\alpha$'s and $\Delta\beta$'s are changes in intramolecular interaction and intermolecular interaction energies in mixing. According to the RIS scheme,[35,36] the unperturbed characteristic ratio is a function of only the intramolecular-interaction energies:

$$\langle r^2\rangle_0/nl^2 = g(\alpha_1, \alpha_2, \alpha_3, ...) \tag{16}$$

Even if different combinations of solvent and temperature yield approximately the same Δw_{12} value and satisfy the condition of the second virial coefficient $A_2 \propto (1/2 - \chi) \approx 0$ (the Θ state), unless almost the same set of α's are obtained, an identical $\langle r^2\rangle_0/nl^2$ value would not be observed from the different systems. Accordingly, it is quite natural that each Θ condition shows its own $\langle r^2\rangle_0/nl^2$ value. For PEO, two interaction energies, E_σ and E_ω, are exceedingly subject to solvent effects and show marked variations with solvent properties.[6,57−59] Therefore, the characteristic ratio represents the environment dependence of the polymer rather than the *characteristic* features of the polymer itself. Some Θ aqueous solutions for PEO include inorganic salts; electrostatic interactions due to the ions affect the hydrogen bonds and chain configuration of PEO. The interactions in these systems are still more complicated. The applicability of the simple expression of eq 13 and the conventional theories based thereon to polymers showing the attractive interactions should be discussed.

Acknowledgment. We thank Dr. Joachim H. G. Steinke of Imperial College, U.K. for hopeful suggestions on synthetic methods of the copolymers. This work was partly supported by the Asahi Glass Foundation and a Grant-in-Aid for Scientific Research (B) (18350112) from the Japan Society for the Promotion of Science.

Appendix. Statistical Weight Matrixes of MEMA (PEIEO) and MEDA (PMEIEO).

Statistical weight matrices, $\mathbf{U}_j^l$ (j, bond number), of the l forms of MEMA and PEIEO were formulated according to the 9×9 scheme:

$$\mathbf{U}_2^l = \begin{bmatrix} 1 & \gamma & \delta \\ 0 & 0 & 0 \\ 0 & 0 & 0 \end{bmatrix} \tag{A1}$$

$$\mathbf{U}_3^l = \begin{bmatrix} 1 & \sigma\nu' & \sigma\eta & 0 & 0 & 0 & 0 & 0 & 0 \\ 0 & 0 & 0 & 1 & \sigma\eta & \sigma\omega & 0 & 0 & 0 \\ 0 & 0 & 0 & 0 & 0 & 0 & 1 & \sigma\omega & \sigma\nu' \end{bmatrix} \tag{A2}$$

$$\mathbf{U}_4^l = \mathbf{U}_c^l = \begin{bmatrix} 1 & \rho & \rho & 0 & 0 & 0 & 0 & 0 & 0 \\ 0 & 0 & 0 & 1 & \rho & \rho\omega' & 0 & 0 & 0 \\ 0 & 0 & 0 & 0 & 0 & 0 & 1 & 0 & \rho \\ 1 & \rho & \rho & 0 & 0 & 0 & 0 & 0 & 0 \\ 0 & 0 & 0 & 1 & \rho & 0 & 0 & 0 & 0 \\ 0 & 0 & 0 & 0 & 0 & 0 & 1 & 0 & \rho \\ 1 & \rho & \rho & 0 & 0 & 0 & 0 & 0 & 0 \\ 0 & 0 & 0 & 1 & \rho & 0 & 0 & 0 & 0 \\ 0 & 0 & 0 & 0 & 0 & 0 & 1 & \rho\omega' & \rho \end{bmatrix} \tag{A3}$$

$$\mathbf{U}_5^l = \mathbf{U}_d^l = \begin{bmatrix} 1 & \rho & \rho & 0 & 0 & 0 & 0 & 0 & 0 \\ 0 & 0 & 0 & 1 & \rho & 0 & 0 & 0 & 0 \\ 0 & 0 & 0 & 0 & 0 & 0 & 1 & 0 & \rho \\ 1 & \rho & \rho & 0 & 0 & 0 & 0 & 0 & 0 \\ 0 & 0 & 0 & 1 & \rho & 0 & 0 & 0 & 0 \\ 0 & 0 & 0 & 0 & 0 & 0 & 1 & 0 & \rho \\ 1 & \rho & \rho & 0 & 0 & 0 & 0 & 0 & 0 \\ 0 & 0 & 0 & 1 & \rho & 0 & 0 & 0 & 0 \\ 0 & 0 & 0 & 0 & 0 & 0 & 1 & 0 & \rho \end{bmatrix} \tag{A4}$$

$$\mathbf{U}_6^l = \mathbf{U}_e^l = \begin{bmatrix} 1 & \sigma & \sigma & 0 & 0 & 0 & 0 & 0 & 0 \\ 0 & 0 & 0 & 1 & \sigma & \sigma & 0 & 0 & 0 \\ 0 & 0 & 0 & 0 & 0 & 0 & 1 & \sigma & \sigma \\ 1 & \sigma & \sigma & 0 & 0 & 0 & 0 & 0 & 0 \\ 0 & 0 & 0 & 1 & \sigma & \sigma & 0 & 0 & 0 \\ 0 & 0 & 0 & 0 & 0 & 0 & 1 & 0 & \sigma \\ 1 & \sigma & \sigma & 0 & 0 & 0 & 0 & 0 & 0 \\ 0 & 0 & 0 & 1 & \sigma & 0 & 0 & 0 & 0 \\ 0 & 0 & 0 & 0 & 0 & 0 & 1 & \sigma & \sigma \end{bmatrix} \tag{A5}$$

$$\mathbf{U}_7^l = \mathbf{U}_f^l = \begin{bmatrix} 1 & \delta & \gamma & 0 & 0 & 0 & 0 & 0 & 0 \\ 0 & 0 & 0 & \eta & \delta\nu' & \gamma\omega & 0 & 0 & 0 \\ 0 & 0 & 0 & 0 & 0 & 0 & \nu' & \delta\omega & \gamma\eta \\ 1 & \delta & \gamma & 0 & 0 & 0 & 0 & 0 & 0 \\ 0 & 0 & 0 & \eta & \delta\nu' & \gamma\omega & 0 & 0 & 0 \\ 0 & 0 & 0 & 0 & 0 & 0 & \nu'\omega' & 0 & 0 \\ 1 & \delta & \gamma & 0 & 0 & 0 & 0 & 0 & 0 \\ 0 & 0 & 0 & 0 & \delta\nu'\omega' & 0 & 0 & 0 & 0 \\ 0 & 0 & 0 & 0 & 0 & 0 & \nu' & \delta\omega & \gamma\eta \end{bmatrix} \tag{A6}$$

$$\mathbf{U}_a^l = \begin{bmatrix} 1 & \gamma & \delta & 0 & 0 & 0 & 0 & 0 & 0 \\ 0 & 0 & 0 & 1 & \gamma & 0 & 0 & 0 & 0 \\ 0 & 0 & 0 & 0 & 0 & 0 & 1 & \gamma\omega'' & \delta \\ 1 & \gamma & \delta & 0 & 0 & 0 & 0 & 0 & 0 \\ 0 & 0 & 0 & 1 & \gamma & 0 & 0 & 0 & 0 \\ 0 & 0 & 0 & 0 & 0 & 0 & 1 & 0 & \delta \\ 1 & \gamma & \delta & 0 & 0 & 0 & 0 & 0 & 0 \\ 0 & 0 & 0 & 1 & \gamma & 0 & 0 & 0 & 0 \\ 0 & 0 & 0 & 0 & 0 & 0 & 1 & \gamma\omega'' & \delta \end{bmatrix} \tag{A7}$$

and

$$\mathbf{U}_b^l = \begin{bmatrix} 1 & \sigma\nu' & \sigma\eta & 0 & 0 & 0 & 0 & 0 & 0 \\ 0 & 0 & 0 & 1 & \sigma\eta & \sigma\omega & 0 & 0 & 0 \\ 0 & 0 & 0 & 0 & 0 & 0 & 1 & \sigma\omega & \sigma\nu' \\ 1 & \sigma\nu' & \sigma\eta & 0 & 0 & 0 & 0 & 0 & 0 \\ 0 & 0 & 0 & 1 & \sigma\eta & \sigma\omega & 0 & 0 & 0 \\ 0 & 0 & 0 & 0 & 0 & 0 & 1 & 0 & \sigma\nu' \\ 1 & \sigma\nu' & \sigma\eta & 0 & 0 & 0 & 0 & 0 & 0 \\ 0 & 0 & 0 & 1 & \sigma\eta & 0 & 0 & 0 & 0 \\ 0 & 0 & 0 & 0 & 0 & 0 & 1 & \sigma\omega & \sigma\nu' \end{bmatrix} \tag{A8}$$

The $\mathbf{U}_j^l$ matrices of the l forms of MEDA and PMEIEO are given as follows:

$$\mathbf{U}_2^l = \begin{bmatrix} 1 & \gamma & 1 \\ 0 & 0 & 0 \\ 0 & 0 & 0 \end{bmatrix} \tag{A9}$$

$$\mathbf{U}_3^l = \begin{bmatrix} 1 & \sigma\nu' & \sigma\omega & 0 & 0 & 0 & 0 & 0 & 0 \\ 0 & 0 & 0 & 1 & \sigma\omega & \sigma\omega & 0 & 0 & 0 \\ 0 & 0 & 0 & 0 & 0 & 0 & 1 & \sigma\omega & \sigma\nu' \end{bmatrix} \tag{A10}$$

The $\mathbf{U}_4^l - \mathbf{U}_6^l$ ($\mathbf{U}_c^l - \mathbf{U}_e^l$) matrices are identical to those of MEMA (PEIEO).

$$\mathbf{U}_7^l = \mathbf{U}_f^l = \begin{bmatrix} 1 & 1 & \gamma & 0 & 0 & 0 & 0 & 0 & 0 \\ 0 & 0 & 0 & \omega & \nu' & \gamma\omega & 0 & 0 & 0 \\ 0 & 0 & 0 & 0 & 0 & 0 & \nu' & \omega & \gamma\omega \\ 1 & 1 & \gamma & 0 & 0 & 0 & 0 & 0 & 0 \\ 0 & 0 & 0 & \omega & \nu' & \gamma\omega & 0 & 0 & 0 \\ 0 & 0 & 0 & 0 & 0 & 0 & \nu'\omega' & 0 & 0 \\ 1 & 1 & \gamma & 0 & 0 & 0 & 0 & 0 & 0 \\ 0 & 0 & 0 & 0 & \nu'\omega' & 0 & 0 & 0 & 0 \\ 0 & 0 & 0 & 0 & 0 & 0 & \nu' & \omega & \gamma\omega \end{bmatrix} \tag{A11}$$

$$\mathbf{U}_a^l = \begin{bmatrix} 1 & \gamma & 1 & 0 & 0 & 0 & 0 & 0 & 0 \\ 0 & 0 & 0 & 1 & \gamma & 0 & 0 & 0 & 0 \\ 0 & 0 & 0 & 0 & 0 & 0 & 1 & \gamma\omega'' & 1 \\ 1 & \gamma & 1 & 0 & 0 & 0 & 0 & 0 & 0 \\ 0 & 0 & 0 & 1 & \gamma & 0 & 0 & 0 & 0 \\ 0 & 0 & 0 & 0 & 0 & 0 & 1 & 0 & 1 \\ 1 & \gamma & 1 & 0 & 0 & 0 & 0 & 0 & 0 \\ 0 & 0 & 0 & 1 & \gamma & 0 & 0 & 0 & 0 \\ 0 & 0 & 0 & 0 & 0 & 0 & 1 & \gamma\omega'' & 1 \end{bmatrix} \tag{A12}$$

and

$$\mathbf{U}_b^l = \begin{bmatrix} 1 & \sigma\nu' & \sigma\omega & 0 & 0 & 0 & 0 & 0 & 0 \\ 0 & 0 & 0 & 1 & \sigma\omega & \sigma\omega & 0 & 0 & 0 \\ 0 & 0 & 0 & 0 & 0 & 0 & 1 & \sigma\omega & \sigma\nu' \\ 1 & \sigma\nu' & \sigma\omega & 0 & 0 & 0 & 0 & 0 & 0 \\ 0 & 0 & 0 & 1 & \sigma\omega & \sigma\omega & 0 & 0 & 0 \\ 0 & 0 & 0 & 0 & 0 & 0 & 1 & 0 & \sigma\nu' \\ 1 & \sigma\nu' & \sigma\omega & 0 & 0 & 0 & 0 & 0 & 0 \\ 0 & 0 & 0 & 1 & \sigma\omega & 0 & 0 & 0 & 0 \\ 0 & 0 & 0 & 0 & 0 & 0 & 1 & \sigma\omega & \sigma\nu' \end{bmatrix} \quad \text{(A13)}$$

The intramolecular interactions adopted here are illustrated in Figures 3, 7, and 8. The statistical weight matrices of the *d* forms can be derived from

$$\mathbf{U}_2^d = \mathbf{Q}_3\mathbf{U}_2^l\mathbf{Q}_3 \quad \text{(A14)}$$

$$\mathbf{U}_3^d = \mathbf{Q}_3\mathbf{U}_3^l\mathbf{Q}_9 \quad \text{(A15)}$$

and

$$\mathbf{U}_j^d = \mathbf{Q}_9\mathbf{U}_j^l\mathbf{Q}_9 \quad \text{(A16)}$$

where $j \geq 4$,

$$\mathbf{Q}_3 = \begin{pmatrix} 1 & 0 & 0 \\ 0 & 0 & 1 \\ 0 & 1 & 0 \end{pmatrix} \quad \text{(A17)}$$

and

$$\mathbf{Q}_9 = \mathbf{Q}_3 \otimes \mathbf{Q}_3 \quad \text{(A18)}$$

References and Notes

(1) Sasanuma, Y. Intramolecular Interactions of Polyethers and Polysulfides, Investigated by NMR, Ab Initio Molecular Orbital Calculations, and Rotational Isomeric State Scheme: An Advanced Analysis of NMR Data. In *Annu. Rep. NMR Spectrosc.*; Webb, G. A. Ed.; Academic Press: New York, 2003; Vol. 49, Chapter 5.
(2) Sasanuma, Y.; Watanabe, A. *Macromolecules* **2006**, *39*, 1646.
(3) Sasanuma, Y.; Kato, H.; Kaito, A. *J. Phys. Chem. B* **2003**, *107*, 11852.
(4) Sasanuma, Y.; Hattori, S.; Imazu, S.; Ikeda, S.; Kaizuka, T.; Iijima, T.; Sawanobori, M.; Azam, M. A.; Law, R. V.; Steinke, J. H. G. *Macromolecules* **2004**, *37*, 9169.
(5) Sasanuma, Y.; Teramae, F.; Yamashita, H.; Hamano, I.; Hattori, S. *Macromolecules* **2005**, *38*, 3519.
(6) Sasanuma, Y.; Ohta, H.; Touma, I.; Matoba, H.; Hayashi, Y.; Kaito, A. *Macromolecules* **2002**, *35*, 3748.
(7) Gray, F. M. *Solid Polymer Electrolytes*: *Fundamentals and Technological Applications*; Wiley & Sons: New York, 1991; Chapter 2.
(8) Boussif, O.; Lezoualc'h, F.; Zanta, M. A.; Mergny, M. D.; Scherman, D.; Demeneix, B.; Behr, J. P. *Proc. Natl. Acad. Sci. U.S.A.* **1995**, *92*, 7297.
(9) Neu, M.; Fischer, D.; Kissel, T. *J. Gene Med.* **2005**, *7*, 992.
(10) Inasmuch as the NMR spectra of the model compounds were observed from organic and fully basic aqueous solutions, the compounds are free from protonation ($-N^+H_2-$ or $-N^+H(CH_3)-$). Therefore, the protonation has not been considered here for the models and polymers.
(11) Vinogradov, S. V.; Bronich, T. K.; Kabanov, A. V. *Bioconjugate Chem.* **1998**, *9*, 805.
(12) Akiyama, Y.; Harada, A.; Nagasaki, Y.; Kataoka, K. *Macromolecules* **2000**, *33*, 5841.
(13) Park, M. R.; Han, K. O.; Han, I. K.; Cho, M. H.; Nah, J. W.; Choi, Y. J.; Cho, C. S. *J. Controlled Release* **2005**, *105*, 367.
(14) Tomalia, D. A.; Ojha, N. D. U.S. Patent 3,752,854, 1973.
(15) Frisch, M. J.; Trucks, G. W.; Schlegel, H. B.; Scuseria, G. E.; Robb, M. A.; Cheeseman, J. R.; Montgomery, J. A., Jr.; Vreven, T.; Kudin, K. N.; Burant, J. C.; Millam, J. M.; Iyengar, S. S.; Tomasi, J.; Barone, V.; Mennucci, B.; Cossi, M.; Scalmani, G.; Rega, N.; Petersson, G. A.; Nakatsuji, H.; Hada, M.; Ehara, M.; Toyota, K.; Fukuda, R.; Hasegawa, J.; Ishida, M.; Nakajima, T.; Honda, Y.; Kitao, O.; Nakai, H.; Klene, M.; Li, X.; Knox, J. E.; Hratchian, H. P.; Cross, J. B.; Bakken, V.; Adamo, C.; Jaramillo, J.; Gomperts, R.; Stratmann, R. E.; Yazyev, O.; Austin, A. J.; Cammi, R.; Pomelli, C.; Ochterski, J. W.; Ayala, P. Y.; Morokuma, K.; Voth, G. A.; Salvador, P.; Dannenberg, J. J.; Zakrzewski, V. G.; Dapprich, S.; Daniels, A. D.; Strain, M. C.; Farkas, O.; Malick, D. K.; Rabuck, A. D.; Raghavachari, K.; Foresman, J. B.; Ortiz, J. V.; Cui, Q.; Baboul, A. G.; Clifford, S.; Cioslowski, J.; Stefanov, B. B.; Liu, G.; Liashenko, A.; Piskorz, P.; Komaromi, I.; Martin, R. L.; Fox, D. J.; Keith, T.; Al-Laham, M. A.; Peng, C. Y.; Nanayakkara, A.; Challacombe, M.; Gill, P. M. W.; Johnson, B.; Chen, W.; Wong, M. W.; Gonzalez, C.; Pople, J. A. *Gaussian 03*, revision C.02; Gaussian, Inc.: Wallingford, CT, 2004.
(16) Pople, J. A.; Scott, A. P.; Wong, M. W.; Radom, L. *Isr. J. Chem.* **1993**, *33*, 345.
(17) Boys, S. F.; Bernardi, F. *Mol. Phys.* **1970**, *19*, 553.
(18) Simon, S.; Duran, M.; Dannenberg, J. J. *J. Chem. Phys.* **1996**, *105*, 11024.
(19) Reed, A. E.; Curtiss, L. A.; Weinhold, F. *Chem. Rev.* **1988**, *88*, 899.
(20) Glendening, E. D.; Reed, A. E.; Carpenter, J. E.; Weinhold, F. *NBO* version 3.1; Theoretical Chemistry Institute and Department of Chemistry, University of Wisconsin: Madison, WI, 1992.
(21) Kudin, K. N.; Scuseria, G. E. *Chem. Phys. Lett.* **1998**, *289*, 611.
(22) Kudin, K. N.; Scuseria, G. E. *Phys. Rev. B* **2000**, *61*, 16440.
(23) Case, D. A.; Darden, T. A.; Cheatham, T. E., III; Simmerling, C. L.; Wang, J.; Duke, R. E.; Luo, R.; Merz, K. M.; Wang, B.; Pearlman, D. A.; Crowley, M.; Brozell, S.; Tsui, V.; Gohlke, H.; Mongan, J.; Hornak, V.; Cui, G.; Beroza, P.; Schafmeister, C.; Caldwell, J. W.; Ross, W. S.; Kollman, P. A. *AMBER 8;* University of California at San Francisco: San Francisco, CA, 2004.
(24) Wang, J.; Cieplak, P.; Kollman, P. A. *J. Comput. Chem.* **2000**, *21*, 1049.
(25) Bayly, C. I.; Cieplak, P.; Cornell, W. D.; Kollman, P. A. *J. Phys. Chem.* **1993**, *97*, 10269.
(26) Vona, M. L. D. Illuminati, G.; Lillocci, C. *J. Chem. Soc., Perkin Trans. 2* **1985**, 1943.
(27) Maeda, H.; Furuyoshi, S.; Nakatsuji, Y.; Okahara, M. *Bull. Chem. Soc. Jpn.* **1983**, *56*, 212.
(28) Cottle, D. L.; Jeltsch, A. E. Stoudt, T. H.; Walters, D. R. *J. Org. Chem.* **1946**, *11*, 286.
(29) Budzelaar, P. H. M. *gNMR*, version 5.0; IvorySoft & Adept Scientific plc: Letchworth, U.K., 2004.
(30) The NMR spectra observed from MEMA dissolved in $(CD_3)_2SO$ and MEDA in all the solvents may be interpreted as simple triplets. Then, we have ${}^3J_{HH} = {}^3J'_{HH}$. If the rotation around the C−C bond is so rapid that all the vicinal couplings are completely equivalent, the coupling constants would be averaged according to

$${}^3J_{HH} = {}^3J'_{HH} = \frac{{}^3J_T^{HH} + {}^3J_G^{HH}}{2}p_t^{CC} + \frac{{}^3J'_T{}^{HH} + {}^3J'_G{}^{HH} + {}^3J''_G{}^{HH} + {}^3J'''_G{}^{HH}}{4}p_g^{CC}$$

This equation gives the p_t^{CC} values for parts b and c of Figure 2 as 0.41 and 0.55, respectively. On the other hand, eqs 1−3 yield the p_t^{CC} values of 0.28 (Figure 2b) and 0.28 (Figure 2c). The latter p_t^{CC} values are close to the MO calculations. As seen from Figure 2b, the $-NHC\underline{H}_2-$ triplet of MEMA is broader than the $-C\underline{H}_2O-$ peaks; the two methylene groups have different relaxation times because association of MEMA with DMSO hinders the internal rotations. Therefore, it is reasonable to adopt eqs 1−3 rather than the above equation. For these NMR observations as well, we have employed eqs 1−3, assuming that ${}^3J_{HH} = {}^3J'_{HH}$.
(31) Inomata, K.; Abe, A. *J. Phys. Chem.* **1992**, *96*, 7934.
(32) The energy was roughly estimated as the sum of bond−antibond, bond−Rydberg, lone pair−antibond, and lone pair−Rydberg interaction energies.
(33) Flory, P. J.; Mark, J. E.; Abe, A. *J. Am. Chem. Soc.* **1966**, *88*, 639.
(34) Flory, P. J. *J. Am. Chem. Soc.* **1967**, *89*, 1798.
(35) Flory, P. J. *Statistical Mechanics of Chain Molecules*; Wiley & Sons: New York, 1969.
(36) Mattice, W. L.; Suter, U. W. *Conformational Theory of Large Molecules*: *The Rotational Isomeric State Model in Macromolecular Systems*; Wiley & Sons: New York, 1994.
(37) Vacatello, M.; Flory, P. J. *Macromolecules* **1986**, *19*, 405.
(38) Mattice, W. L.; Helfer, C. A.; Sokolov, A. P. *Macromolecules* **2004**, *37*, 4711.
(39) Bunn, C. W. *Trans. Faraday Soc.* **1939**, *35*, 482.
(40) Kobayashi, S.; Tadokoro, H.; Chatani, Y. *Makromol. Chem.* **1968**, *112*, 225.
(41) Imada, K.; Miyakawa, T.; Chatani, Y.; Tadokoro, H.; Murahashi, S. *Makromol. Chem.* **1965**, *83*, 113.
(42) Tadokoro, H.; Chatani, Y.; Yoshihara, T.; Tahara, S.; Murahashi, S. *Makromol. Chem.* **1964**, *73*, 109.

(43) Takahashi, Y.; Tadokoro, H. *Macromolecules* **1973**, *6*, 672.
(44) Takahashi, Y.; Sumita, I.; Tadokoro, H. *J. Polym. Sci., Polym. Phys. Ed.* **1973**, *11*, 2113.
(45) Tashiro, K.; Tadokoro, H. *Rep. Prog. Poly. Phys. Jpn.* **1978**, *21*, 417.
(46) Chatani, Y.; Kobatake, T.; Tadokoro, H.; Tanaka, R. *Macromolecules* **1982**, *15*, 170.
(47) Hydrogen atoms were attached to the terminals of the helical chains optimized by the MO calculation under the periodic condition, and the NBO analysis using the 6-31G(d) basis set was performed.
(48) (a) Chatani, Y.; Tadokoro, H.; Saegusa, T.; Ikeda, H. *Macromolecules* **1981**, *14*, 315. (b) Chatani, Y.; Kobatake, T.; Tadokoro, H. *Macromolecules* **1983**, *16*, 199.
(49) Hashida, T.; Tashiro, K.; Aoshima, S.; Inaki, Y. *Macromolecules* **2002**, *35*, 4330.
(50) Núñez, A.; Berroterán, D.; Núñez, O. *Org. Biomol. Chem.* **2003**, *1*, 2283.
(51) Griffiths, P. C.; Paul, A.; Stilbs, P.; Petterson, E. *Macromolecules* **2005**, *38*, 3539.
(52) Love, P.; Cohen, R. B.; Taft, R. W. *J. Am. Chem. Soc.* **1968**, *90*, 2455.
(53) Tanaka, R.; Ueoka, I.; Takaki, Y.; Kataoka, K.; Saito, S. *Macromolecules* **1983**, *16*, 849.
(54) (a) Saegusa, T.; Ikeda, H.; Fujii, H. *Polym. J.* **1972**, *3*, 35. (b) Saegusa, T.; Ikeda, H.; Fujii, H. *Macromolecules* **1972**, *5*, 108.
(55) Saegusa, T.; Nagura, Y.; Kobayashi, S. *Macromolecules* **1973**, *6*, 495.
(56) Flory, P. J. *Principles of Polymer Chemistry*; Cornell University Press: Ithaca, NY, 1953; Chapter 12.
(57) Baldwin, D. T.; Mattice, W. L.; Gandour, R. D. *J. Comput. Chem.* **1984**, *5*, 241.
(58) Abe, A.; Furuya, H.; Mitra, M. K.; Hiejima, T. *Comput. Theor. Polym. Sci.* **1998**, *8*, 253.
(59) Smith, G. D.; Bedrov, D.; Borodin, O. *J. Am. Chem. Soc.* **2000**, *122*, 9548.

MA0612531